© 2015. Published by The Company of Biologists Ltd | Development (2015) 142, 3921-3932 doi:10.1242/dev.124271

RESEARCH ARTICLE

Aspm sustains postnatal cerebellar neurogenesis and medulloblastoma growth in mice

Scott E. Williams[1,2,¶,§], Idoia Garcia[3,*,‡,§], Andrew J. Crowther[3,4], Shiyi Li[3], Alyssa Stewart[3], Hedi Liu[3], Kendall J. Lough[1], Sean O'Neill[3], Katherine Veleta[3,4], Esteban A. Oyarzabal[3,4], Joseph R. Merrill[5], Yen-Yu Ian Shih[3,4,5,6] and Timothy R. Gershon[2,3,4,¶]

ABSTRACT

Alterations in genes that regulate brain size may contribute to both microcephaly and brain tumor formation. Here, we report that *Aspm*, a gene that is mutated in familial microcephaly, regulates postnatal neurogenesis in the cerebellum and supports the growth of medulloblastoma, the most common malignant pediatric brain tumor. Cerebellar granule neuron progenitors (CGNPs) express Aspm when maintained in a proliferative state by sonic hedgehog (Shh) signaling, and Aspm is expressed in Shh-driven medulloblastoma in mice. Genetic deletion of *Aspm* reduces cerebellar growth, while paradoxically increasing the mitotic rate of CGNPs. *Aspm*-deficient CGNPs show impaired mitotic progression, altered patterns of division orientation and differentiation, and increased DNA damage, which causes progenitor attrition through apoptosis. Deletion of *Aspm* in mice with Smo-induced medulloblastoma reduces tumor growth and increases DNA damage. Co-deletion of *Aspm* and either of the apoptosis regulators *Bax* or *Trp53* (also known as *p53*) rescues the survival of neural progenitors and reduces the growth restriction imposed by *Aspm* deletion. Our data show that Aspm functions to regulate mitosis and to mitigate DNA damage during CGNP cell division, causes microcephaly through progenitor apoptosis when mutated, and sustains tumor growth in medulloblastoma.

KEY WORDS: CGNPs, Cerebellar neurogenesis, Medulloblastoma, Microcephaly, Mitosis, Division orientation

INTRODUCTION

Microcephaly syndromes may provide clues for identifying genetic targets for brain tumor therapy. During brain development, proliferation of transient-amplifying cells generates appropriately sized populations of different types of neurons. In primary microcephaly, impaired progenitor amplification produces a developmental outcome whereby the overall brain size is markedly reduced, but the diversity of cell types is preserved (Woods et al., 2005). Mutations found in microcephaly may indicate genes required by transient-amplifying cells. Because specific brain tumors grow as transient-amplifying cells, disrupting microcephaly genes may produce a clinically useful anti-tumor effect.

The microtubule-associated centrosomal protein ASPM (abnormal spindle microcephaly-associated) has been implicated in both primary microcephaly and cancer. Mutations in human *ASPM* occur in familial microcephaly (Bond et al., 2002, 2003; Woods et al., 2005), and studies in model organisms have shown that ASPM is expressed by neural stem cells and promotes brain growth (Bond et al., 2002; Pulvers et al., 2010; Marinaro et al., 2011; Rujano et al., 2013). ASPM has also been implicated in the growth of diverse cancers, including medulloblastomas (Vulcani-Freitas et al., 2011), gliomas (Horvath et al., 2006; Bikeye et al., 2010), hepatocellular carcinomas (Lin et al., 2008), ovarian cancers (Brüning-Richardson et al., 2011) and pancreatic cancers (Wang et al., 2013). Thus, loss of *Aspm* function is associated with growth failure, and aberrant ASPM is associated with excessive growth.

Various functions of ASPM have been identified that may support proliferation. In *Drosophila*, *asp* maintains mitotic spindle orientation during both mitosis and meiosis (Zhong et al., 2005; van der Voet et al., 2009; Kaindl et al., 2010; Rujano et al., 2013). In mice, *Aspm* is required to maintain spindle organization and positioning and acts as a microtubule-organizing center in telencephalic neuroepithelial progenitors (Fish et al., 2006; Higgins et al., 2010). Asp and Aspm are expressed at centrosomes and spindle midbody microtubules, and their loss causes defects in spindle assembly and mitotic progression (Saunders et al., 1997; Wakefield et al., 2001; Fish et al., 2006; van der Voet et al., 2009; Pulvers et al., 2010; Novorol et al., 2013). Aspm might also play a role in DNA double-strand break repair through non-homologous end joining (Kato et al., 2011). The net effect of these diverse functions is promotion of proliferation, but it remains unclear how these functions converge.

The postnatal cerebellum presents an opportunity to study Aspm function in both developmental brain growth and tumorigenesis. Cerebellar growth is typically reduced in primary microcephaly (Adachi et al., 2014), whereas medulloblastoma, the most common malignant pediatric brain tumor, is a neoplastic overgrowth of the cerebellum. Postnatal CGNP proliferation drives cerebellar growth. This proliferation lasts through the first 2 weeks of life in mice or first year of life in humans, generating the largest population of neurons in the brain. During this period, CGNPs proliferate in the external granule layer (EGL) of the cerebellum. Actively cycling CGNPs are $PCNA^+$ and typically reside in the outer zone (oEGL), whereas postmitotic CGNPs express Cdkn1b (p27) and accumulate in the inner zone (iEGL). From the iEGL, postmitotic CGNPs migrate through the molecular layer (ML) into the internal granule layer (IGL) where they complete differentiation to become granule

[1]Department of Pathology & Laboratory Medicine, University of North Carolina School of Medicine, Chapel Hill, NC 27599, USA. [2]Lineberger Comprehensive Cancer Center, University of North Carolina School of Medicine, Chapel Hill, NC 27599, USA. [3]Department of Neurology, University of North Carolina School of Medicine, Chapel Hill, NC 27599, USA. [4]UNC Neuroscience Center, University of North Carolina School of Medicine, Chapel Hill, NC 27599, USA. [5]Biomedical Research Imaging Center, University of North Carolina, Chapel Hill, NC 27599, USA. [6]Department of Biomedical Engineering, University of North Carolina, Chapel Hill, NC 27599, USA.
*Present address: Neuro-Oncology Group, Biodonostia Institute, San Sebastián, Spain. ‡Present address: IKERBASQUE, Basque Foundation for Science, Bilbao, Spain.
§These authors contributed equally to this work

¶Authors for correspondence (scott_williams@med.unc.edu; gershont@neurology.unc.edu)

Received 12 March 2015; Accepted 28 September 2015

Development (2015) 142, 3921-3932 doi:10.1242/dev.124271

neurons (GNs) (Hatten et al., 1982; Roussel and Hatten, 2011; Hibi and Shimizu, 2012).

Postnatal CGNP proliferation depends on mitogenic signaling from locally secreted Shh (Dahmane and Ruiz-i-Altaba, 1999; Wechsler-Reya and Scott, 1999; Kenney and Rowitch, 2000). Shh pathway activation is found in 25% of medulloblastoma patients including 65% of patients younger than 2 or older than 16 years (Zurawel et al., 2000a,b; Ellison et al., 2011; Northcott et al., 2011). In genetically engineered mice, Shh pathway hyperactivation in CGNPs produces malignant cerebellar tumors that resemble human SHH subtype medulloblastomas, providing *in vivo* models of medulloblastoma tumorigenesis (Zurawel et al., 2000a,b; Hallahan et al., 2004; Schüller et al., 2008; Yang et al., 2008) and metastasis (Hatton et al., 2008).

Here, we show that Aspm plays an essential role in CGNP proliferation, differentiation and survival in mice. Genetic deletion of *Aspm* reveals important functions in mitotic progression, maintenance of CGNP position and orientation during mitosis, and mitigation of proliferation-dependent DNA damage. Deletion of *Aspm* increases DNA damage and induces progenitor apoptosis that depends on Bax and p53. Aspm expression persists in Shh-driven medulloblastomas in transgenic mice, where these functions support tumor growth.

RESULTS

Aspm is induced by Shh and upregulated during cerebellar neurogenesis

Aspm is expressed at major sites of postnatal neurogenesis in the brain. At postnatal day (P) 7, the peak of CGNP proliferation, *Aspm* mRNA localized predominantly to the oEGL (Fig. 1A). We mapped Aspm expression and postnatal neurogenesis by injecting P6 *Aspm-GFP* reporter mice with 5-ethynyl-2′-deoxyuridine (EdU) and harvesting brains 24 h later. GFP expression corresponded with sites of proliferation indicated by EdU, including the EGL and subventricular zone (SVZ; Fig. 1B). Widefield (Fig. 1C) and confocal (Fig. 1D) microscopy demonstrated GFP throughout the EGL in P7 *Aspm-GFP* mice, including differentiating iEGL cells. In light of our *in situ* hybridization data, we attribute the persistent GFP signal in the iEGL to stability of the GFP protein beyond its period of transcription. Like *Aspm* mRNA, GFP reporter fluorescence waned by P16 (Fig. 1E), following the temporal pattern of CGNP proliferation (Fujita, 1967). The relationship between *Aspm* expression and CGNP proliferation was further demonstrated by real-time, quantitative PCR (RT-qPCR). *Aspm* expression was relatively high at the peak of neurogenesis (P7) and waned by P16 (Fig. 1F), mirroring the expression of cyclin D2 (*Ccnd2*), a previously identified marker of CGNP proliferation (Kenney and Rowitch, 2000).

We examined the relationship between Shh signaling and Aspm expression in isolated, freshly explanted CGNPs. Shh-supplemented CGNPs *in vitro* expressed >4-fold more *Aspm* mRNA compared with Shh-deprived CGNPs (Fig. 1G). Shh signaling is transduced by Smoothened (Smo) and can be blocked by the Smo inhibitor vismodegib (Rubin and de Sauvage, 2006). CGNPs treated with Shh+vismodegib expressed Aspm similarly to Shh-deprived CGNPs (Fig. 1G). CGNPs from *Aspm-GFP* mice expressed robust GFP when cultured with Shh and downregulated GFP when Shh-deprived (Fig. 1H). These findings show that Aspm expression is integral to the Shh-driven CGNP proliferation program.

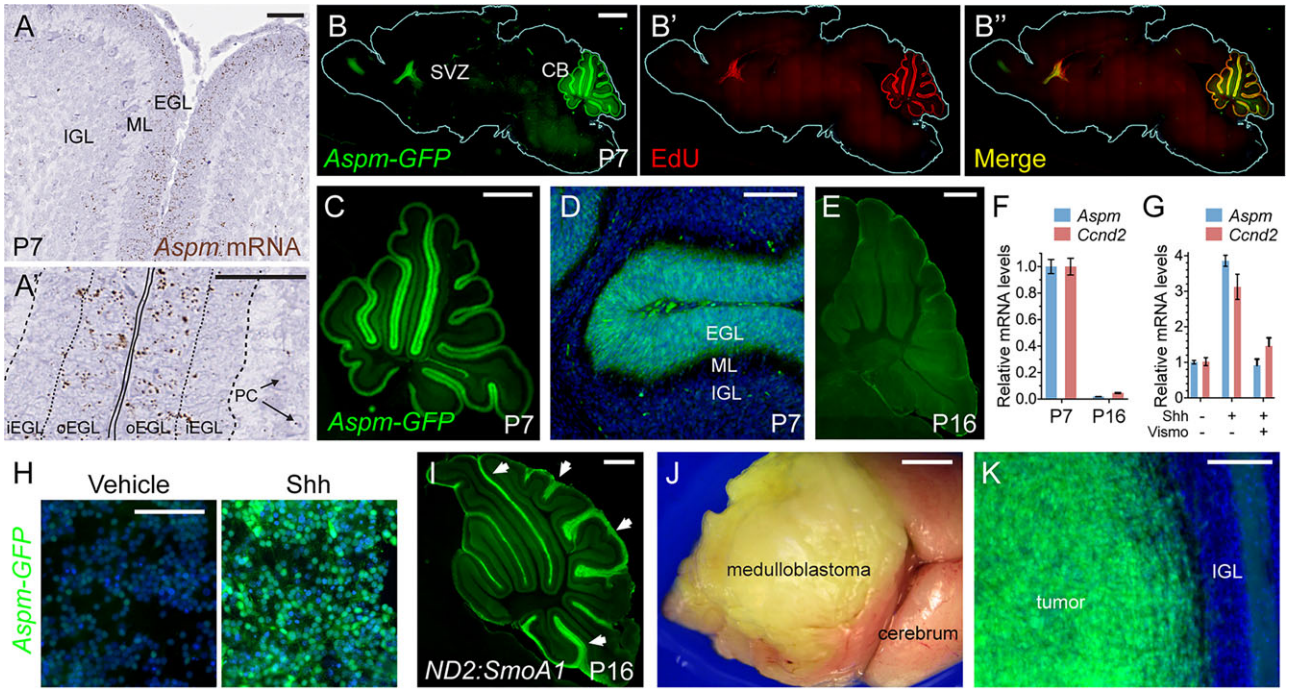

Fig. 1. Aspm expression in the postnatal cerebellum. (A,A′) P7 *in situ* hybridization demonstrates *Aspm* mRNA primarily in the oEGL. PC, Purkinje cell. (B-B″) Sagittal section of P7 *Aspm-GFP* mouse brain injected at P6 with EdU shows GFP expression in EdU^{+} zones of postnatal neurogenesis, the cerebellum (CB) and SVZ. (C-E) GFP fluorescence in *Aspm-GFP* cerebella at P7 (C, high magnification in D) and P16 (E). (F) RT-qPCR quantification of *Aspm* and *Ccnd2*, normalized to *Gapdh*, during (P7) and after (P16) CGNP proliferation. (G) Shh induced a ~4- to 5-fold increase in *Aspm* and *Ccnd2* mRNAs *in vitro* that was blocked by vismodegib. (H) Isolated CGNPs from *Aspm-GFP* mice express GFP only when cultured with Shh. (I) Sagittal cerebellar section of a *ND2:SmoA1; Aspm-GFP* mouse shows continued expression of GFP at P16, in contrast to the wild-type *Aspm-GFP* cerebellum shown in E. White arrowheads indicate the persistent EGL resulting from sustained Shh activity. (J,K) Medulloblastomas in *ND2:SmoA1;Aspm-GFP* mice express GFP specifically in tumor cells. Scale bars: 100 µm (A,D,H,K); 1 mm (B,J); 500 µm (C,E,I).

Development (2015) 142, 3921-3932 doi:10.1242/dev.124271

To determine whether Shh hyperactivation induces Aspm *in vivo*, we crossed *Aspm-GFP* reporter mice with the transgenic, medulloblastoma-prone *ND2:SmoA1* mouse line, which expresses a constitutively active allele of *Smo* under control of the *NeuroD2* promoter. CGNPs of *ND2:SmoA1* mice show cell-autonomous Shh-pathway activation, prolonged CGNP proliferation, and predisposition to medulloblastoma (Hallahan et al., 2004). In *Aspm-GFP;ND2:SmoA1* mice, CGNPs proliferated beyond the typical 15-day period, and expressed *Aspm-GFP* uniformly throughout the aberrantly persistent EGL (Fig. 1I). In spontaneous medulloblastomas, GFP was consistently and homogeneously expressed (n>15; Fig. 1J,K). Although not specifically implicating components of the Shh pathway as transcriptional regulators of Aspm, these data show that Shh signaling through Smo was necessary to maintain Aspm expression *in vitro* and is sufficient to drive Aspm expression *in vivo*, as an integral part of the Shh-driven proliferative program in both persistent CGNPs and Shh-driven medulloblastomas in *ND2:SmoA1* mice.

To examine the fate of Aspm-expressing postnatal progenitors, we generated *Aspm-CreER;Rosa26-Lox-STOP-Lox-tdTomato* mice, which express a tamoxifen-inducible red fluorescent reporter controlled by the *Aspm* promoter (Marinaro et al., 2011). Mice were harvested at P11 following tamoxifen injection at P4 and P7. Red fluorescence was observed in neurogenic regions throughout the brain (Fig. 2A), including neural progenitors in the rostral migratory stream (Fig. 2B), hippocampus (Fig. 2C; Fig. S1D,E) and EGL (Fig. 2D,E). TdTomato also labeled differentiated neurons in the cerebellum, including interneurons (Fig. 2E and Fig. S1B, yellow arrowheads) and GNs, identified by their position in the IGL and colocalization with NeuN (Rbfox3 – Mouse Genome Informatics) (Fig. 2F; Fig. S1A,B). In the ML, tdTomato and NeuN co-labeled differentiating CGNPs migrating to the IGL (Fig. 2G and Fig. S1A, red arrowheads). In addition, tdTomato$^+$ tubular structures throughout the brain expressed the endothelial marker CD31 (Pecam1 – Mouse Genome Informatics), identifying them as capillaries (Fig. 2E and Fig. S1A‴,C, blue arrowheads). No tdTomato$^+$ cells expressed the glial marker GFAP, which labels Bergmann glia and astrocytes (Fig. 2H; Fig. S2F). Thus, Aspm$^+$ progenitors in the postnatal brain gave rise to CGNPs (identified by their position in the EGL), differentiated neurons, and capillary endothelial cells, with minimal glial progeny.

Aspm is required for cerebellar growth

To determine whether Aspm function is required for CGNP proliferation, we generated and analyzed *Aspm*^{SA} mice, which harbor a splice-acceptor and *lacZ*-neomycin cassette into the intron between exons 6 and 7 (see supplementary Materials and Methods; Fig. S2A). We verified *Aspm* deficiency in *Aspm*$^{SA/SA}$ mice by RT-qPCR, which demonstrated an absence of full-length *Aspm* mRNA in *Aspm*$^{SA/SA}$ cerebella, compared with *Aspm*$^{SA/+}$ littermates (Fig. 3A). *Aspm*$^{SA/SA}$ males were sterile, like the *Aspm*-deficient males previously described (Pulvers et al., 2010). Because of the complex geometry of the brain, we used brain weight to detect changes in size. Whole brains and dissected cerebella of *Aspm*$^{SA/SA}$ mice were significantly smaller than brains and cerebella of *Aspm*$^{SA/+}$ or *Aspm*$^{+/+}$ littermates (Fig. 3B,C). These results show that the *Aspm*$^{SA/SA}$ mouse line phenocopies previously reported *Aspm* mutant mice (Pulvers et al., 2010), and that *Aspm* deficiency reduced the size of the cerebellum along with the rest of the brain.

To determine whether Aspm is specifically required by CGNPs, we generated an *Aspm* conditional allele (Aspm^f; Fig. S2B) by crossing *Aspm*$^{SA/SA}$ and *Rosa26-FLPe* (Farley et al., 2000) mouse lines. We then used Cre-mediated recombination to delete *Aspm* conditionally in the Math1 (Atoh1 – Mouse Genome Informatics) lineage (Fig. S2B,C), which in the cerebellum is restricted to CGNPs (Helms et al., 2000; Machold and Fishell, 2005; Matei et al., 2005). The resulting *Math1-Cre;Aspm*$^{f/f}$ mice (*Aspm* cKO), expressed less *Aspm* mRNA in cerebella, compared with *Aspm*$^{f/f}$ littermates without Cre (Fig. 3A). Although overall brain weight was preserved in *Aspm* cKO mice owing to limited expression of

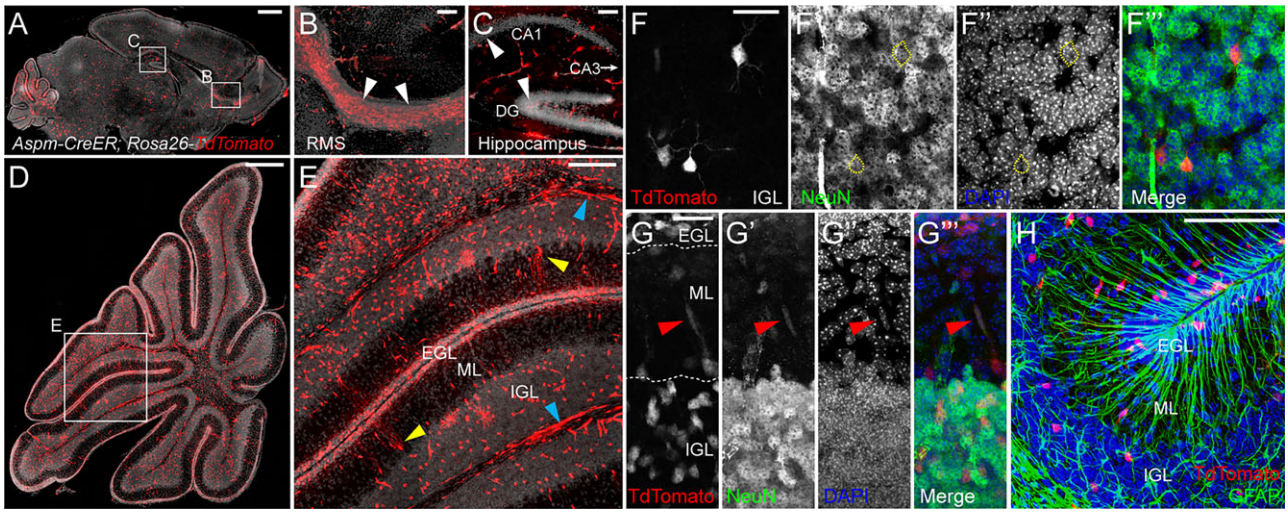

Fig. 2. Lineage tracing of *Aspm*-expressing descendants in the cerebellum. (A-E) Sagittal P11 brain section from a representative *Aspm-CreER;tdTomato* reporter mouse injected with tamoxifen (at P4 and P7) showing red fluorescence in progenitor regions including the cerebellum, rostral migratory stream (RMS; B) and dentate gyrus (DG; C). Arrowheads indicate TdTomato$^+$ neural progenitors. (D,E) Aspm lineage within the cerebellum includes CGNPs, GNs, interneurons [yellow arrowheads, probably Lugaro cells (Schilling et al., 2008)] and endothelial cells (blue arrowheads). (F-G‴) Single plane (F-F‴) and maximum projection (G-G‴) confocal images of P7 *Aspm-CreER;tdTomato* mice injected with tamoxifen at P4. TdTomato$^+$ mature GNs in the IGL (yellow dashed outline in F′,F″) are NeuN$^+$. TdTomato/NeuN double-positive cells are found in the IGL as well as migrating in the ML (red arrowheads in G-G‴). Dashed lines in G mark the border between cerebellar layers. (H) Absence of colocalization of the glial marker GFAP and TdTomato. Scale bars: 1 mm (A): 200 µm (B,C); 500 µm (D) 100 µm (E,H); 25 µm (F,G).

Development (2015) 142, 3921-3932 doi:10.1242/dev.124271

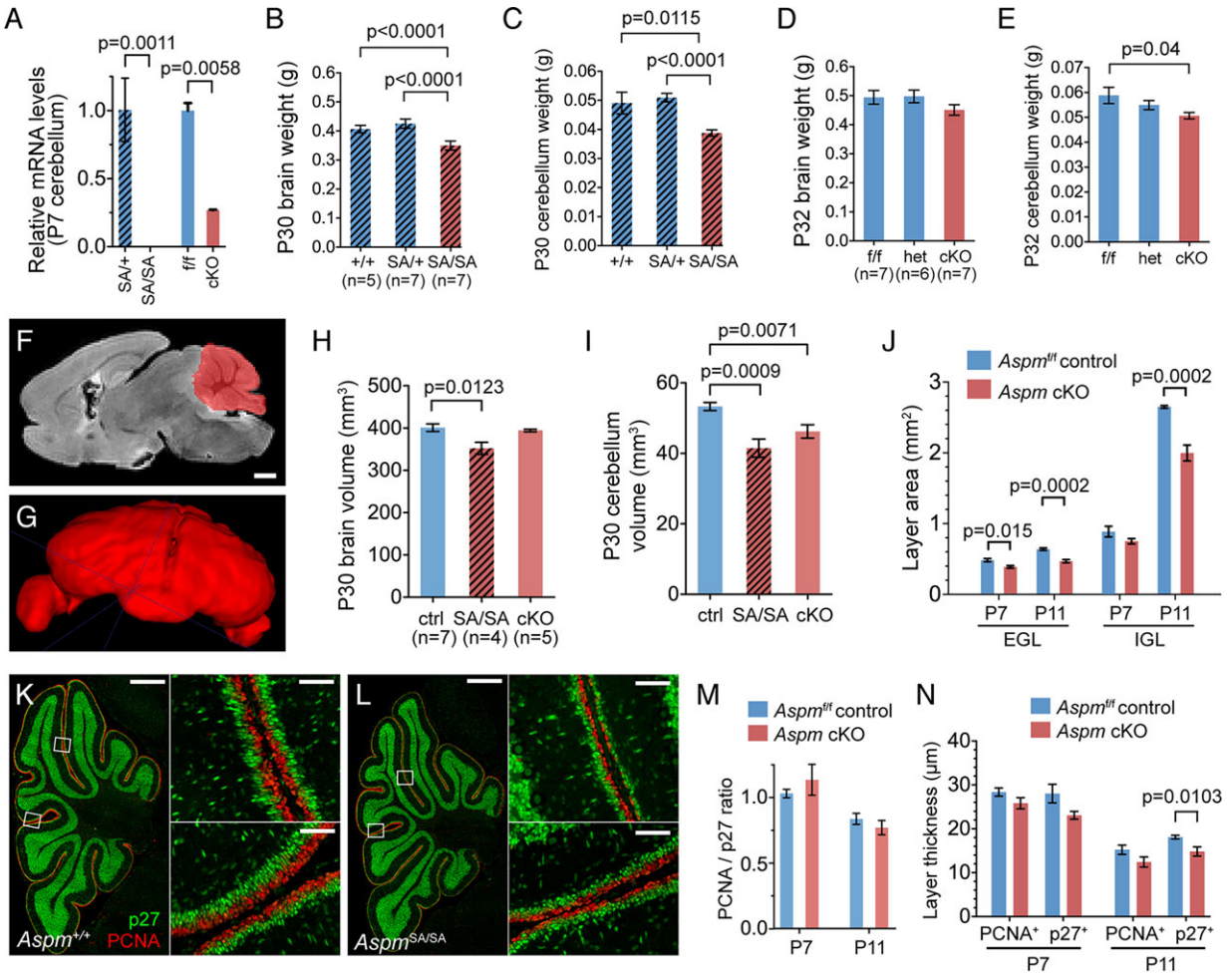

Fig. 3. *Aspm* deletion and reduced brain growth in *Aspm*$^{SA/SA}$ and *Aspm* cKO mice. (A) RT-qPCR shows reduced *Aspm* mRNA in *Aspm*$^{SA/SA}$ and *Aspm* (*Math1-Cre*) cKO cerebella (*n*=3). Residual mRNA in *Aspm* cKO cerebella is due to cells outside the *Math1* lineage. (B,C) Brain and cerebella weight were significantly decreased in *Aspm*$^{SA/SA}$ mice compared with both *Aspm*$^{SA/+}$ and *Aspm*$^{+/+}$ littermates. (D,E) Cerebellum weight was significantly decreased in *Aspm* cKO mice compared with littermate no-Cre (f/f) and *Math1-Cre;Aspm*$^{f/+}$ (het) controls; overall brain weight was unaffected. (F) Sagittal MRI of *Aspm* cKO brain with cerebellum shaded in red. (G) Three-dimensional reconstruction of cKO cerebellum from MRI data, showing normal gross morphology. (H,I) MRI volume measurements of brain (H) and cerebellum (I) show reduced growth in *Aspm*$^{SA/SA}$ brains and in *Aspm*$^{SA/SA}$ and *Aspm* cKO cerebella. (J) EGL area is significantly reduced in *Aspm* cKOs at both P7 and P11, with IGL area also decreasing at P11. (K,L) Representative P11 sagittal cerebellar sections show reduced EGL thickness in *Aspm*$^{SA/SA}$ mice (L) compared with wild-type littermates (K). High magnification of boxed areas are shown on the right. (M) Ratio of PCNA$^+$:p27$^+$ areas is not significantly different in *Aspm* cKOs at P7 and P11. (N) Thinning of the p27$^+$ iEGL was statistically significant at P11. Scale bars: 1 mm (F); 250 μm (K,L); 50 μm (K,L insets).

Math1-Cre outside the cerebellum (Fig. 3D), cerebellum weight was significantly reduced compared with littermate controls (Fig. 3E). We also measured the volume of intact, unprocessed brains using magnetic resonance imaging (MRI), and used manual segmentation to determine the volume of the cerebellum (Fig. 3F-I; Movies 1, 2). Consistent with weight measurements, MRIs showed reduced brain and cerebellum volume in *Aspm*$^{SA/SA}$ mutants, and reduced cerebellar volume in *Aspm* cKOs. The smaller cerebellum in the cKO demonstrates a cell-autonomous requirement for *Aspm* in CGNPs to maintain normal cerebellar growth.

We next sought to determine the onset of growth restriction observed in *Aspm* cKOs. The EGL typically thins between P7 and P15 as proliferation wanes, whereas the IGL grows as GNs populate it. Measurements of EGL and IGL area at P7 and P11 showed that both regions were significantly smaller in *Aspm* cKOs, with the most significant difference between genotypes occurring in the IGL at P11 (Fig. 3J). Thus, in *Aspm* cKOs, the thinning of the EGL was accelerated and the growth of the IGL reduced.

The organization of the EGL was largely preserved in cerebella of *Aspm* cKOs, with the PCNA$^+$ oEGL and post-mitotic, p27$^+$ iEGL present at similar ratios as in controls (Fig. 3K,L). In littermate controls at P7, the ratio of the area of the PCNA$^+$ region to the p27$^+$ region was 1.031±0.032 (mean±s.e.m.), decreasing to 0.838±0.043 by P11 as proliferation wanes. In *Aspm* cKOs from P7 to P11, the PCNA:p27 ratio decreased more rapidly, from 1.135±0.12 to 0.771±0.054 (Fig. 3M). Comparison of the thickness of the oEGL (PCNA$^+$) and iEGL (p27$^+$) layers between cKOs and controls showed that each layer grew progressively thinner in cKOs, with the most significant difference occurring in the iEGL at P11 (Fig. 3N). These data suggest a defect in the differentiating population of CGNPs in the Aspm cKOs that becomes progressively more evident over time.

Aspm cKO CGNPs show hyperproliferation and mitotic defects

To determine whether *Aspm* deficiency decreased the mitogenic response of CGNPs to Shh, we compared proliferation in CGNPs

Development (2015) 142, 3921-3932 doi:10.1242/dev.124271

isolated from either *Aspm* cKO mice or *Aspm*$^{f/f}$ littermates, cultured with or without Shh for 48 h by counting mitotic figures, identified by immunofluorescence labeling for phospho-histone H3 (pHH3). This comparison showed that although Shh increased the mitotic rate of both genotypes, cKO CGNPs demonstrated significantly more mitoses (Fig. 4A,B). Thus, *in vitro*, Shh-induced proliferation was increased, rather than decreased, by *Aspm* deficiency.

To compare the proliferation rate of CGNPs *in vivo*, we counted mitoses along the entire length of the EGL in midline sagittal sections of P5 *Aspm* cKO mice and *Aspm*$^{f/f}$ littermate controls (n=6 per genotype). We identified mitotic cells by co-immunofluorescence for pHH3, which marks prophase-early anaphase, and survivin (Birc5 – Mouse Genome Informatics), which localizes to the midbody region and cleavage furrow during anaphase-telophase (Caldas et al., 2005; Williams et al., 2011). To control for differences in EGL thickness between controls and cKOs, we normalized mitotic cell counts to EGL area to determine the mitotic rate across the entire EGL population. Using these criteria, we noted a significant increase in overall mitotic rates in the *Aspm* cKO EGL (Fig. 4C,D), consistent with our *in vitro* data and with previous observations in zebrafish *aspm* mutants (Kim et al., 2011; Novorol et al., 2013).

The spatial pattern of mitoses was disrupted by *Aspm* deficiency. Because all mitotic cells are expected to be PCNA/Ki67^{+}, we used spatial criteria, rather than PCNA and p27 (as in Fig. 3) to define EGL layers. We considered the superficial EGL (EGL$_S$) to extend from the pial surface inwards to 50% of EGL depth, and the deep EGL (EGL$_D$) to extend from the midway point to the inner EGL margin. At the ages examined (P5-P7), this demarcation approximates but does not exactly correspond with the border of the oEGL, defined by expression of PCNA or Ki67 (Mki67 – Mouse Genome Informatics), both of which extend over half the thickness of the EGL (Fig. S3F,G).

We measured the position of all pHH3^{+} cells in the EGL at P5 relative to the pia mater (Fig. S3A,B). Mitotic figures tended to occur further from the pia in cKOs compared with *Aspm*$^{f/f}$ littermates (Fig. S3C; n>3000 cells/genotype). In controls, ~80% of mitoses occurred in the EGL$_S$, consistent with previous observations (79.6%) in rat EGL (Zagon and McLaughlin, 1987). By contrast, in cKOs, the proportion of mitoses occurring in the

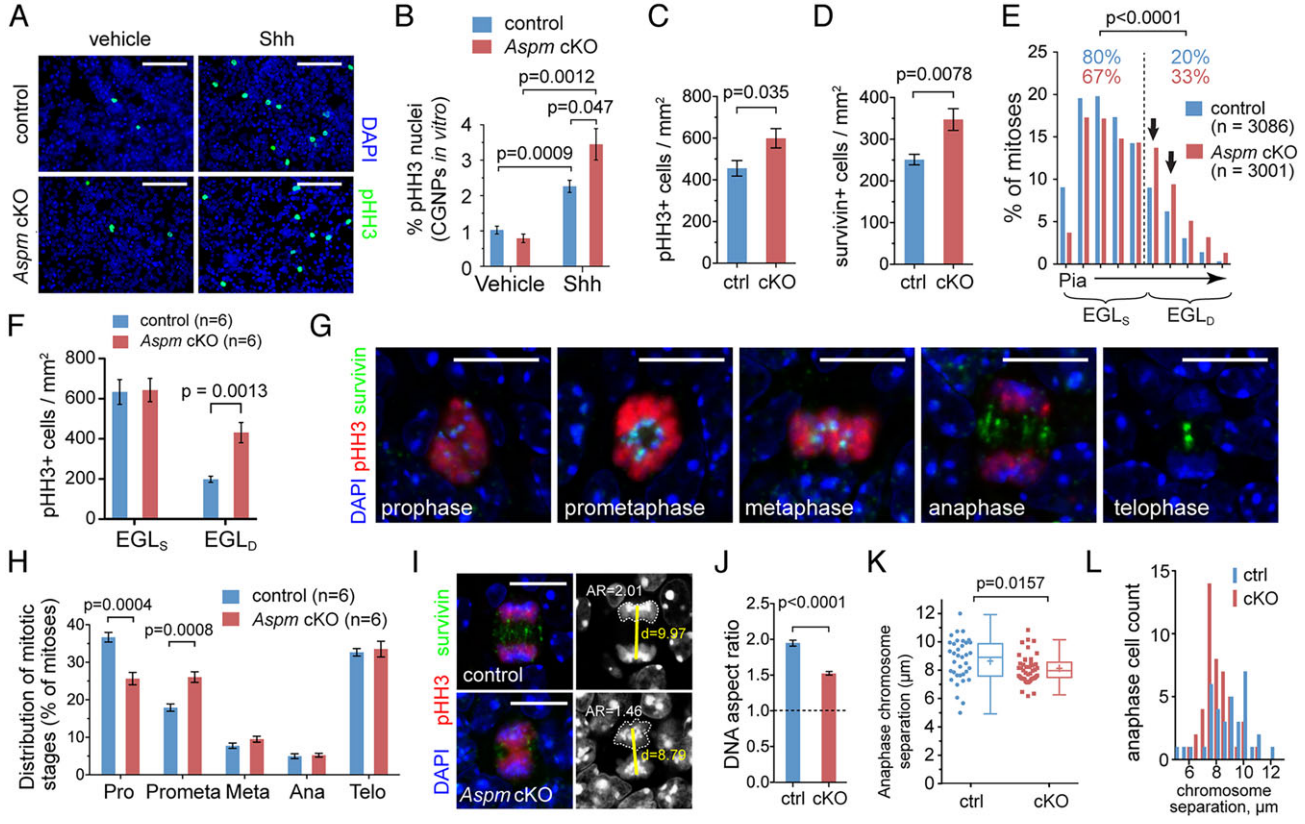

Fig. 4. *Aspm*-deficient CGNPs show mitotic defects. (A,B) pHH3 immunofluorescence shows Shh-induced proliferation of cKO and control CGNPs *in vitro*. (C,D) *In situ*, the density of both early stage pHH3^{+} and late-stage survivin^{+} mitotic cells in the EGL was significantly elevated in *Aspm* cKOs. (E) Histogram showing frequency of mitoses by position within the EGL at P5, binned by 10% increments of EGL thickness. Compared with controls, a greater proportion of mitoses occurred farther from the pia in the EGL$_D$ in *Aspm* cKOs. Dashed line demarcates the midpoint of the EGL; arrows indicate the bins (50-60%, 60-70%) with the greatest increase in mitotic figures in cKOs. Blue and red figures indicate the percentage of mitoses falling within each bin. (F) Quantification of pHH3^{+} density in superficial (EGL$_S$) and deep (EGL$_D$) regions showing an increase in supernumerary mitoses specifically within the EGL$_D$ in *Aspm* cKOs. (G) pHH3 and survivin identify CGNPs at specific phases of mitosis. Prophase cells are weakly pHH3^{+} and are survivin^{-}; prometaphase and metaphase cells are strongly pHH3^{+} with survivin^{+} on kinetochores; metaphase DNA shows a characteristic bar shape; anaphase cells are weakly pHH3^{+} and are survivin^{+} in the spindle midbody; telophase cells are pHH3^{-} with intense punctate survivin staining around the cleavage furrow. (H) A significant reduction in prophase and increase in prometaphase cells is observed in *Aspm* cKOs. (I-L) Anaphase chromosome morphology. (I) Representative images of *Aspm*$^{f/f}$ (top) and cKO (bottom) anaphase cells, showing where the DNA aspect ratio (AR) and inter-chromosome distance (d) were measured. (J) Control anaphase chromosomes were significantly rounder (lower AR) than wild-type counterparts, which adopt a characteristic bar shape. Dot plot and box-and-whisker plots (K) and histogram (L) of inter-chromosome distance. *Aspm* cKOs showed a spike at intermediate distances, suggesting a delay in anaphase progression. Scale bars: 100 μm (A); 10 μm (G,I). *P* values determined by two-tailed Student's *t*-tests except those in E (χ^2) and K (Mann–Whitney).

Development (2015) 142, 3921-3932 doi:10.1242/dev.124271

EGL_S was reduced to ~67% (Fig. 4E). Normalizing cell counts to either EGL area (Fig. 4F) or length (Fig. S3D,E), we found similar mitotic frequency in the EGL_S of both genotypes, but significantly increased mitotic frequency in the EGL_D in cKOs. Co-labeling with $pHH3^+$ and either Ki67 or PCNA to mark the proliferative oEGL, showed that >90% of mitoses occurred within the $Ki67/PCNA^+$ domains, with no statistically significant difference between genotypes (Fig. S3F-H). Importantly, all mitotic cells outside of these domains (Fig. S3F,G, arrowheads) were $PCNA^+$ or $Ki67^+$ as expected. Thus, spatial measurement revealed differences in the position of mitoses that could not be determined by analysis of marker expression. In the independent cohort used for co-labeling with Ki67 or PCNA, we again observed a significant increase in $pHH3^+$ figures in the cKO compared with controls (Fig. S3I), predominantly localized to the EGL_D (Fig. 4F; Fig. S3J). As shown in Fig. 4E (arrows), the greatest increase in mitotic figures in cKOs was observed in the 50th-70th percentile of EGL thickness near the EGL_S/EGL_D boundary.

Because Asp/Aspm have been reported to play a role in mitotic spindle assembly and function (Wakefield et al., 2001; Riparbelli et al., 2002; Paramasivam et al., 2007), we used chromosome morphology and pHH3/survivin co-immunofluorescence to determine the distribution of mitotic stages found in wild-type and *Aspm* cKO CGNPs (Fig. 4G). We noted a decrease in the proportion of prophase cells and an increase in the proportion of prometaphase cells in cKOs relative to $Aspm^{f/f}$ controls (Fig. 4H). This altered distribution at early mitosis suggests that *Aspm* loss impairs mitotic progression at the time the spindle is forming. We also noted that *Aspm*-deficient CGNPs displayed abnormal rounded DNA during anaphase, suggestive of defects in organizing the spindle poles, whereas $Aspm^{f/f}$ control CGNPs showed a more typical bar shape (Fig. 4I,J). The median distance between anaphase chromosome pairs was also significantly shorter in *Aspm* cKOs compared with wild-type controls (Fig. 4K; Mann–Whitney test, $P=0.0157$). Moreover, whereas wild-type cells showed a Gaussian distribution of inter-chromosome distances (Shapiro–Wilk normality test, $P=0.6824$), this distribution was not maintained in cKOs ($P=0.0241$). A disproportionately high percentage of *Aspm* cKO chromosome pairs were separated by 7.5-8.0 µm (Fig. 4L; $n=21/46$ cells examined compared with 9/37 controls). This altered distribution suggests a delay in the transition between anaphase-A, during which chromosome separation is driven by destruction of sister-chromatid adhesion complexes, and anaphase-B, during which the mitotic spindle is elongated as the spindle poles pull the chromosomes apart. Overall, these data support a role for Aspm in promoting mitotic spindle assembly and progression through metaphase into anaphase.

Aspm loss leads to alterations in division orientation and cell cycle exit kinetics

Aspm (Asp) has been implicated in the maintenance of cleavage plane orientation in *Drosophila* neural progenitors (Rujano et al., 2013) though an analogous role for Aspm in mouse is controversial (Fish et al., 2006; Pulvers et al., 2010). In the developing cerebellum, CGNPs adopt different cleavage plane orientations depending on their position within the EGL (Zagon and McLaughlin, 1987). In the EGL_S, CGNPs more frequently orient their spindle perpendicular to the pial surface, whereas CGNPs dividing in the EGL_D more often divide either parallel or transverse to the pial surface (Zagon and McLaughlin, 1987). Conditional deletion of *Aspm* produced significant changes in the orientation and distribution of divisions within the EGL. The incidence of transverse divisions in *Aspm* cKO CGNPs was increased at the expense of perpendicular divisions (Fig. 5A,B; χ^2 test, $P<0.0001$). Analysis of division orientation relative to EGL depth demonstrated a bias in control cerebella towards perpendicular divisions in the EGL_S (56.1%, $n=301$), with roughly equal frequencies of perpendicular, transverse and parallel divisions in the EGL_D ($n=149$), consistent with prior studies (Zagon and McLaughlin, 1987). This orientation bias was lost in *Aspm* cKOs, in which CGNP division orientation appeared randomized (Fig. 5C). These data provide the first evidence that division orientation in the cerebellum is under molecular control, regulated at least in part by *Aspm*.

To determine whether alterations in division orientation and mitotic progression caused by *Aspm* mutation affected the tendency of CGNPs to re-enter or to exit the cell cycle (e.g. self-renew or differentiate), we examined the fate of CGNPs 24 h or 48 h after injection of 5-bromo-2′-deoxyuridine (BrdU) at P5. We used co-labeling with BrdU and the differentiation marker p27 to determine the proportions of BrdU-labeled cells that either continued or exited the cell cycle (Fig. 5D-K). CGNPs in the EGL were labeled with BrdU with similar frequency at the 24 h time point in $Aspm^{f/f}$ control and cKOs (Fig. 5L), suggesting that CGNPs in both genotypes enter S phase with similar frequency. However, there was a tendency towards fewer actively cycling ($p27^-$) and more differentiating ($p27^+$) $BrdU^+$ CGNPs in the cKOs compared with controls (Fig. 5L). Further analysis showed that a greater proportion of $p27^+$ CGNPs in the iEGL were labeled with BrdU in cKOs compared with controls (Fig. 5M). We quantified the cell cycle exit fraction (proportion of $BrdU^+$ CGNPs in the EGL that were $p27^+$) for both genotypes and found that a greater proportion of $BrdU^+$ cells had exited the cell cycle in *Aspm* cKOs at both the 24 h and 48 h time points (Fig. 5N). In addition, the differentiation index, a measure of the number of $p27^+$ cells produced per $p27^-$ CGNP, was significantly higher in *Aspm* cKOs (Fig. 5O). Finally, we noted a consistent decrease in terminally differentiated $p27^+/BrdU^+$ GNs in the IGL in *Aspm* cKOs, and an increase in $p27^+/BrdU^+$ CGNPs in the EGL at 48 h (Fig. 5P). Together, these data demonstrate that *Aspm* cKO CGNPs prematurely exit the cell cycle but fail to populate the IGL as effectively as normal CGNPs.

Aspm deficiency increases progenitor DNA damage and apoptosis

The overproduction of $p27^+$ CGNPs in the EGL coupled with underproduction of mature GNs in the IGL suggests that *Aspm* cKO CGNPs exhibit either delayed migration or impaired survival. We found no evidence of migration defects as similar numbers of $BrdU^+/p27^+$ neurons were found in the molecular layer in both genotypes at both time points (Fig. 5P). Therefore, we analyzed cell death in the EGL of cKOs and controls by immunohistochemistry for cleaved caspase-3 (cC3) and terminal deoxynucleotidyl transferase dUTP nick end labeling (TUNEL) staining. Apoptosis is rarely detected in the EGL of wild-type mice (Garcia et al., 2012). By contrast, $cC3^+$ cells were significantly increased in the $Aspm^{SA/SA}$ and *Aspm* cKO EGL (Fig. 6A-C) and were proportional to proliferation, i.e. highest at P7 and lower at P11. Similar results were obtained with TUNEL (Fig. 6D). Although apoptotic cells were rare in controls, they were most frequently observed in the EGL_S (86.7±1.2%), whereas in *Aspm* cKOs the density of $cC3^+$ or $TUNEL^+$ apoptotic cells in the EGL_D was increased ~5- to 7-fold over controls (Fig. 6E,F). Thus, apoptosis increased in *Aspm* cKOs in both the proliferating and differentiating populations of CGNPs, with the largest relative increase in the differentiating population. This increase in apoptosis specifically in the EGL_D could explain why fewer mature GNs are produced in *Aspm* cKOs despite the increased production of $p27^+$ CGNPs.

Development (2015) 142, 3921-3932 doi:10.1242/dev.124271

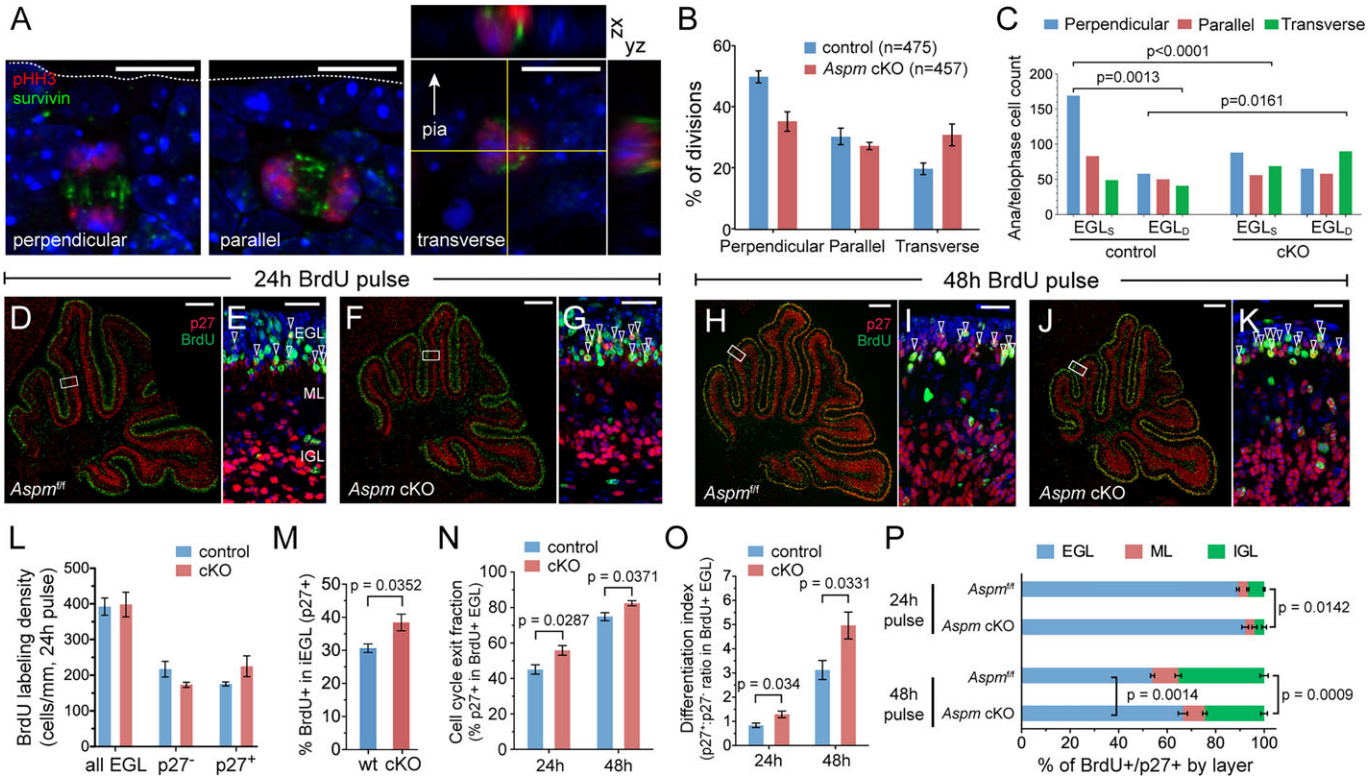

Fig. 5. Division orientation and differentiation are altered in *Aspm* cKOs. (A) Examples of anaphase CGNPs in sagittal sections, oriented with their division plane perpendicular (left), parallel (middle) or transverse (right). *xz* and *yz* projections at the positions indicated by the yellow line are shown for a transverse cell, which divides along the mediolateral axis. Dotted line and arrow indicate the pial surface. (B) Quantification of division orientation for P5 cerebella (n=3 per genotype, 2 sections/cerebellum), with total number of cells analyzed indicated. χ^2 analyses of the proportions of each division type showed a significant difference between control (*Aspm*$^{f/f}$) and cKOs (P<0.0001). (C) Division orientation quantified in the EGL_S and EGL_D. The perpendicular bias in the EGL_S of controls is lost in *Aspm* cKOs. (D-K) p27 (red) and BrdU (green) labeling in control and cKO cerebella following a 24 h (D-G) or 48 h (H-K) BrdU pulse at P5. E, G, I and K are high magnification images of boxed areas in D, F, H and J, respectively. Arrowheads indicate p27$^+$/BrdU$^+$ EGL CGNPs, which are increased in cKOs. (L) Twenty-four hours after injection, similar numbers of CGNPs in the EGL incorporated BrdU, with a trend towards cell cycle exit in the *Aspm* cKO. (M) The percentage of non-proliferative p27$^+$ cells labeled with BrdU following a 48 h pulse is increased in *Aspm* cKOs. (N) Increased cell cycle exit fraction (percentage of BrdU$^+$ cells in EGL that are p27$^+$) in *Aspm* cKO. (O) Increased differentiation index (p27$^+$ CGNPs produced per BrdU-labeled p27$^-$ cell in EGL) in *Aspm* cKOs. (P) Distribution of p27$^+$/BrdU$^+$ cells in the EGL, ML and IGL showed fewer BrdU$^+$ GNs in the cKO IGL (compared with control IGL) both 24 h and 48 h after injection, increased BrdU$^+$p27$^+$ cells in the cKO EGL at 48 h, and no change in the ML. Scale bars: 10 µm (A); 250 µm (D,F,H,J); 25 µm (E,G,I,K). *P* values in C,M,N,O from two-tailed Student's *t*-tests.

CGNPs are highly sensitive to apoptosis in response to genotoxic stress (Chong et al., 2000; Lee et al., 2012). The mitotic abnormalities in *Aspm*-deficient CGNPs, and prior studies demonstrating a role for *Aspm* in mitotic spindle dynamics (Zhong et al., 2005; Fish et al., 2006; Higgins et al., 2010) and DNA repair (Kato et al., 2011) suggest that increased CGNP apoptosis in *Aspm* mutants might be caused by increased DNA damage. Immunolabeling for the DNA damage marker γH2AX demonstrated small, relatively faint γH2AX$^+$ foci in the EGL of all genotypes, and larger foci that were more intense and less frequent. Co-labeling with γH2AX and BrdU, 2 h after BrdU injection, demonstrated that DNA damage was enriched in CGNPs undergoing DNA replication (Fig. 6G). In both *Aspm*$^{SA/SA}$ and *Aspm* cKO mice, γH2AX$^+$ CGNPs were more frequent compared with *Aspm*-intact controls (Fig. 6H-J). These findings implicate DNA damage as a potential mechanism of increased progenitor apoptosis in *Aspm*-deficient mice.

Deletion of key regulators of apoptosis rescues Aspm-induced microcephaly

To determine the contribution of genotoxic stress and progenitor death to growth restriction in *Aspm*-deficient mice, we investigated whether genetic deletions that interrupt the link between DNA damage and apoptosis could rescue the growth of *Aspm*-deficient cerebella. In neural progenitors, DNA damage activates p53, which triggers Bax-dependent apoptosis (Vousden and Lu, 2002; Fridman and Lowe, 2003; Lee and McKinnon, 2007; Crowther et al., 2013). We examined how co-deletion of either *Bax* or *Trp53* affected the *Aspm* cKO phenotype. Because p53 may exert gene dosage-related effects, we selected *Math1-Cre;Aspm*$^{f/f}$*;Trp53*$^{+/+}$ (*Aspm* cKO) and *Math1-Cre;Aspm*$^{f/f}$*;Trp53*$^{f/f}$ (*Aspm;Trp53* dKO) littermates for comparison. For Bax studies, we compared littermates with genotypes *Math1-Cre;Aspm*$^{f/f}$*;Bax*$^{f/f}$ (*Aspm;Bax* dKO), *Math1-Cre;Aspm*$^{f/+}$*;Bax*$^{f/+}$ and *Aspm*$^{f/f}$*;Bax*$^{f/f}$ without Cre. Double mutants and controls were harvested at P30 for comparison of cerebellar weight, or at P7 for comparison of mitosis, DNA damage and apoptosis.

Compared with deletion of *Aspm* alone, cerebellum weight was significantly increased by co-deletion of *Bax* or *Trp53* (Fig. 7A-D). Volumetric MRI confirmed that *Aspm;Bax* dKO cerebella did not exhibit the growth restriction observed in *Aspm* single mutants, and were similar in volume to *Aspm*-intact controls (Fig. 7E). Histological examination, however, showed focal areas of thinning in the IGL in each of the three *Aspm;Bax* dKO cerebella

Development (2015) 142, 3921-3932 doi:10.1242/dev.124271

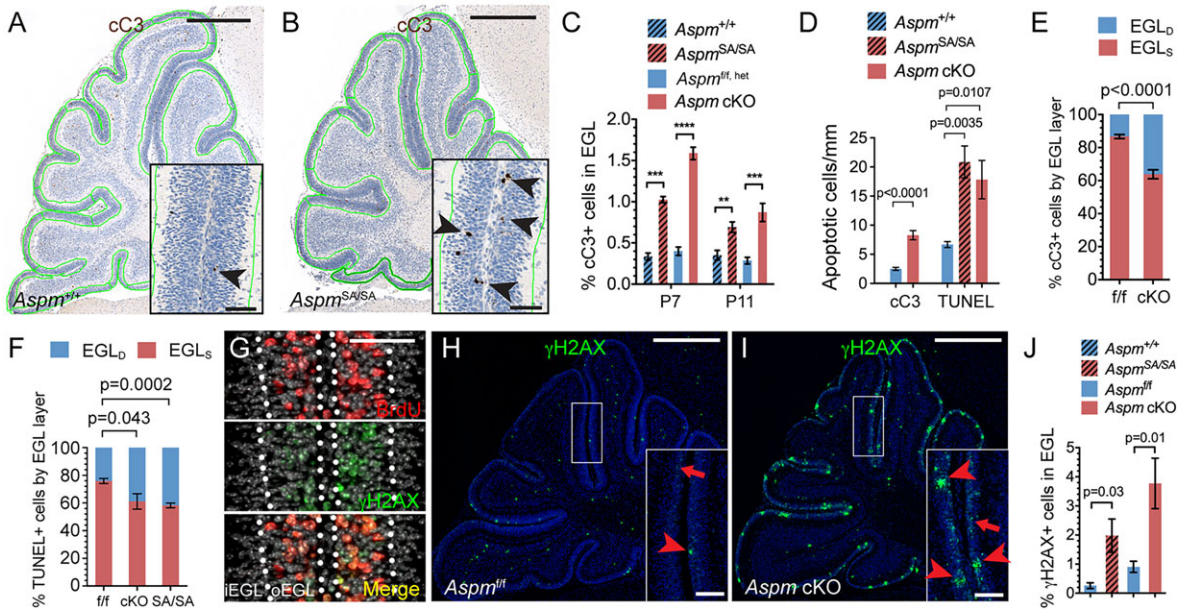

Fig. 6. *Aspm* disruption increases CGNP apoptosis and DNA damage. (A,B) Representative P7 sagittal sections from $Aspm^{+/+}$ (A) and $Aspm^{SA/SA}$ (B) cerebella stained for cC3 (black arrowheads). (C) Quantification of $cC3^+$ cells in the EGL of $Aspm^{SA/SA}$, *Aspm* cKOs, and control littermates demonstrates statistically significant increase in cell death with *Aspm* deficiency. (D) Increased apoptotic cell density ($cC3^+$ or $TUNEL^+$ cells/mm of EGL) in *Aspm* mutants. (E,F) The most significant increase in cell death in *Aspm* mutants, detected by cC3 (E) or TUNEL (F) occurs in differentiating cells of the EGL_D. (G) In control P7 mice, γH2AX$^+$ cells occur primarily in the oEGL and largely overlap with the $BrdU^+$ proliferating population. (H,I) Immunofluorescence for γH2AX in P7 $Aspm^{f/f}$ controls and *Aspm* cKOs. Red arrowheads indicate intense γH2AX$^+$ cells and arrows indicate the presence of γH2AX$^+$ foci. (J) Statistically significant increase in γH2AX$^+$ cells in cKOs at P7. Scale bars: 500 µm (A,B,H,I); 50 µm (A,B,H,I, insets); 50 µm (G).

examined (Fig. 7A,B), though quantification of mean cell density over a broad area of the IGL in replicate sections did not show a statistically significant difference (Fig. 7F). These focal areas of IGL thinning were not observed in *Aspm* cKOs, (data not shown) or in our prior studies of *Bax* single mutants (Garcia et al., 2012). As in *Aspm* single mutants, we noted an increase in mitotic rate across the EGL in each of the double mutants (Fig. 7G). Like *Aspm* single mutants, *Aspm;Bax* and *Aspm;Trp53* mutants showed an elevated percentage of cells at prometaphase and a reduction in prophase (Fig. 7H), demonstrating impaired cell cycle progression. These

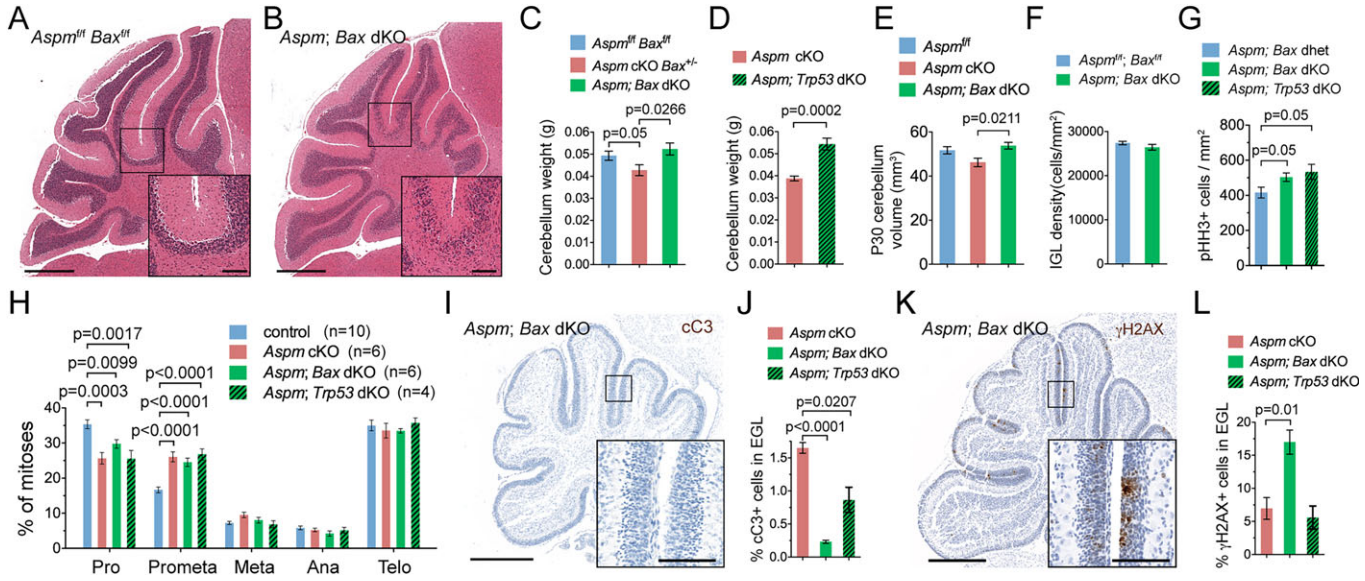

Fig. 7. Co-deletion of *Bax* or *Trp53* with *Aspm* restored cerebellar growth and reduced apoptosis. (A,B) P30 H&E stains show that *Aspm;Bax* dKO cerebellar anatomy is similar to $Aspm^{f/f}$;$Bax^{f/f}$ controls, but with focal areas of abnormally thin IGL (inset). (C,D) Quantification of cerebellum weight in *Aspm;Bax* and *Aspm;Trp53* dKOs, showing a normalization to control levels in the double mutants. (E,F) Cerebellar size, measured by volumetric MRI (E) and IGL cell density, determined by automated counting of nuclei (F) are similar in *Aspm;Bax* dKOs and wild-type controls. (G) Quantification of $pHH3^+$ cells shows that mitotic activity is increased in *Bax;Aspm* and *Trp53;Aspm* double mutants, as in *Aspm* cKOs (Fig. 4E,F). (H) Both double mutants at P7 show a decrease in prophase and increase in prometaphase cells compared with controls, as in *Aspm* cKOs. (I,J) Reduced apoptosis in P7 *Aspm;Bax* double mutants (compare with Fig. 6A,B). (K,L) DNA damage (γH2AX) persists or is increased in both double mutants. Scale bars: 500 µm; 50 µm (insets).

Development (2015) 142, 3921-3932 doi:10.1242/dev.124271

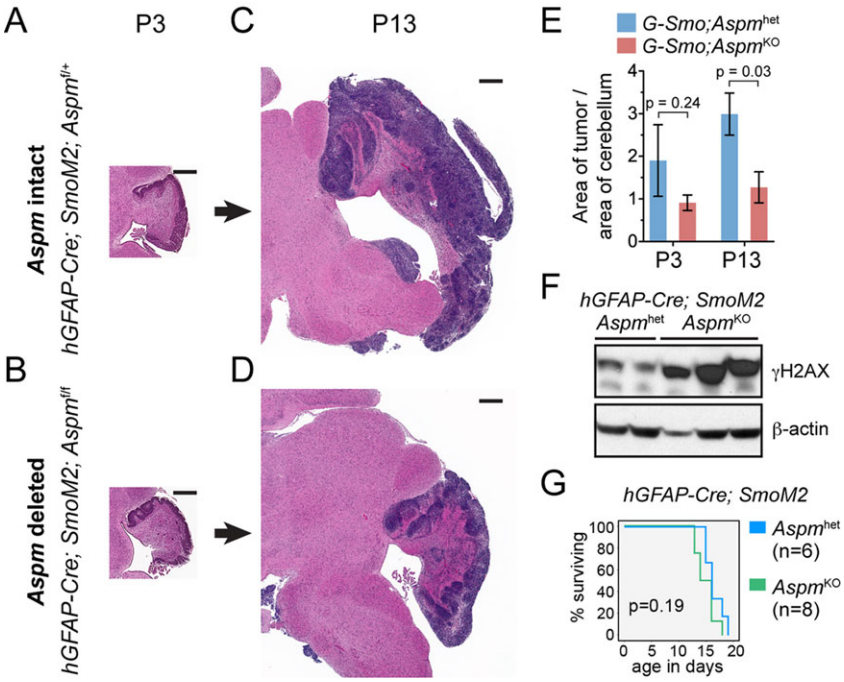

Fig. 8. Conditional deletion of *Aspm* in medulloblastoma slows tumor growth. (A-D) H&E sections of cerebellum (pink) and tumors (purple) at P3 (A,B) and P13 (C,D) in *G-Smo;Aspm*^{het} (A,C) and *G-Smo;Aspm*^{KO} (B,D) mice. (E) Tumor cross-sectional area was significantly reduced by P13 in *G-Smo;Aspm*^{KO} tumors (n=4) compared with *G-Smo;Aspm*^{het} (n=3) littermate tumors. (F) Western blot for γH2AX shows consistently increased levels of DNA damage in *Aspm*-deficient tumors in *G-Smo;Aspm*^{KO} mice at P3. (G) Despite differences in tumor growth rates, Kaplan–Meier curves and log-rank analysis do not demonstrate a statistically significant difference in survival. Scale bars: 500 µm.

abnormalities might underlie the failure of *Bax* co-deletion to completely normalize the cerebellum.

At P7, in both *Aspm;Bax* and *Aspm;Trp53* dKO mice, apoptosis was significantly reduced compared with *Aspm* cKOs (Fig. 7I,J), although DNA damage persisted (Fig. 7K,L). Thus, loss of either *Bax* or *Trp53* led to increased tolerance of DNA damage and reduced cell death, significantly restoring cerebellar growth. The lack of cell death in *Aspm;Bax* dKO mice confirms that the cell death induced by *Aspm* deletion is apoptotic. Focal hypoplasia within the IGL of *Aspm;Bax* dKOs, however, demonstrates that blocking apoptosis did not completely normalize the phenotype of *Aspm* mutation.

Aspm deficiency slows the growth of medulloblastoma

Because Aspm is upregulated in medulloblastoma in both *ND2:SmoA1* mice (Fig. 1I) and patient-derived samples (Vulcani-Freitas et al., 2011), we examined whether Aspm function is essential for tumor growth. We bred *Aspm*$^{f/f}$ mice into the rapidly tumorigenic medulloblastoma model, *hGFAP-Cre;SmoM2* (G-Smo). G-Smo mice express a constitutively active allele of the Shh receptor component Smo (Mao et al., 2006) in stem cells that give rise to the neurons and glia of the cerebrum and cerebellum excluding the Purkinje cells (Zhuo et al., 2001; Kuang et al., 2012), and develop medulloblastoma with 100% incidence, dying of tumor progression by P20 (Schüller et al., 2008). We investigated the effect of *Aspm* deletion on tumor growth by comparing G-Smo mice with *Aspm*$^{f/f}$ (*G-Smo;Aspm*^{KO}) and *Aspm*$^{f/+}$ (*G-Smo;Aspm*^{het}) genotypes.

G-Smo;Aspm^{KO} medulloblastomas grew significantly more slowly than *G-Smo;Aspm*^{het} tumors, although the rate of tumor formation was 100% in both genotypes. Tumors could be differentiated from normal brain in Hematoxylin & Eosin (H&E)-stained sections by their characteristic histology (supplemental Materials and Methods). To compare tumor size, we measured tumor cross-sectional area, normalized to the cross-sectional area of non-tumor cerebellum. At P3, tumor size appeared to be similar in *G-Smo;Aspm*^{KO} (n=4) or *G-Smo;Aspm*^{het} (n=3) mice, and none of the mice showed hydrocephalus (Fig. 8A,B). At P13, however, tumors in *G-Smo;Aspm*^{het} mice had expanded, producing obstructive hydrocephalus, whereas tumors in *G-Smo;Aspm*^{KO} mice (n=4 both genotypes) were significantly smaller and did not develop hydrocephalus (Fig. 8C-E). Within tumors of both genotypes, γH2AX^{+} cells were too numerous and densely packed to be counted. Using western blot, however, we consistently found significantly increased γH2AX^{+} cells in *Aspm*-deleted tumors at P3 (Fig. 8F). By P13, γH2AX^{+} abundance was equivalent (data not shown), suggesting that tumors had developed a mechanism to compensate for *Aspm* deletion.

Despite decreased tumor growth and absence of hydrocephalus, cerebellar anatomy and function was severely disrupted in *G-Smo;Aspm*^{KO} mice. These mice demonstrated severe motor deficits and could not transition from nursing to autonomous feeding, failed to maintain weight on weaning, and required euthanasia to prevent animal suffering. Although *G-Smo;Aspm*^{KO} mice did not seem to die from tumor expansion, because of the motor deficits, *G-Smo;Aspm*^{KO} mice did not survive longer than *G-Smo;Aspm*^{het} controls (Fig. 8G). Although we could not detect a survival benefit in this model, *Aspm* deletion effectively impaired tumor growth.

DISCUSSION

Our studies demonstrate that Aspm plays an essential role in postnatal neurogenesis, and that this role is co-opted in malignant proliferation in medulloblastoma. Aspm is integral to the proliferative program induced in CGNPs by Shh signaling and remains upregulated in Shh-driven medulloblastomas. Conditional deletion of *Aspm* in CGNPs is sufficient to impair cerebellar growth. This growth impairment cannot be attributed to decreased proliferation, as the frequency of CGNP mitosis is actually increased in *Aspm* cKOs. Rather, we show that growth impairment results from a combination of mitotic defects, precocious differentiation, increased DNA damage and increased apoptosis. The increase in proliferation rates in *Aspm* mutants might represent compensatory proliferation, a phenomenon that has been recently described in *Drosophila* centrosomal mutants, which also show spindle assembly defects, elevated DNA damage and increased apoptosis (Poulton et al., 2014).

Development (2015) 142, 3921-3932 doi:10.1242/dev.124271

Apoptosis of *Aspm*-deleted CGNPs was prevented by co-deletion of *Bax* or *Trp53*, which significantly but incompletely restored cerebellar growth. The normalization of cerebellar weight and size in mice with co-deletion of *Aspm* and either *Bax* or *Trp53* demonstrates that preventing apoptosis can largely rescue *Aspm*-dependent growth restriction. The persistent focal abnormalities in the IGL of *Aspm;Bax* dKO mice, however, show that apoptosis is not the only process determining growth failure.

Along with increased DNA damage and apoptosis, we note impaired mitotic progression, changes in the radial position and orientation of mitotic cells, and abnormal patterns of differentiation in *Aspm* cKOs. This raises the intriguing question of whether the heterogeneity in division orientation we and others (Zagon and McLaughlin, 1987) observe in the EGL reflects different modes of division. Recent work has shown that both self-renewing CGNPs and differentiating CGNPs predominantly divide symmetrically (Espinosa and Luo, 2008; Nakashima et al., 2015). Division orientation might influence whether symmetric divisions result in self-renewal or differentiation, such that perpendicular divisions, which are most common in the EGL_D, may promote continued proliferation, whereas transverse orientations, which are elevated in the *Aspm* cKO may promote cell cycle exit.

Human and mouse studies have shown that diverse mutations including *Nde1*, *Cdk5rap2* and *Magoh* induce microcephaly through a combination of loss of progenitor self-renewal, premature differentiation, and progenitor apoptosis (Pawlisz et al., 2008; Lizarraga et al., 2010; Silver et al., 2010; Houlihan and Feng, 2014). Mutations of both *Nde1* and *Cenpj* have been shown to induce microcephaly through p53-dependent apoptosis (Bazzi and Anderson, 2014; Houlihan and Feng, 2014). In all of these examples, the phenotype produced in mice is severe brain malformation. In both our studies and prior investigations, however, *Aspm* deletion produced a phenotype in mice that is much less severe than the orthologous phenotype in humans (Pulvers et al., 2010). Of interest, the microcephaly genes *ASPM* and *CDK5RAP2* have been found to undergo positive selection in primates that correlates with increased brain size (Montgomery and Mundy, 2014); thus, Aspm appears to be particularly important in large-brained animals. We propose that *Aspm* loss impedes brain growth by impairing transient-amplifying cells in a manner that is proportional to the requirement for amplification. Accordingly, *Aspm* deletion is more deleterious in humans, in which brain size is larger and the period of neurogenesis is more prolonged. We have previously shown that a very low rate of apoptosis can exert a significant impact on cerebellar growth, detectable only by comparing growth in apoptosis-deficient, *Bax*-deleted mice (Garcia et al., 2012). A small increase in the rate of progenitor apoptosis may thus produce a significant reduction in brain growth that becomes more pronounced as the proliferation period is extended.

The restriction of tumor growth in *Aspm*-deleted medulloblastoma is consistent with our model in which the effect of *Aspm* loss is proportional to the extent of proliferation. In both cerebellar development and medulloblastoma formation, *Aspm* deletion increased DNA damage. In tumors, however, where proliferation is more extensive than in normal tissues, DNA damage and growth restriction with *Aspm* loss were most pronounced. Importantly, previous investigators have demonstrated that *Aspm* knockdown impairs DNA repair after ionizing radiation *in vitro* (Kato et al., 2011). Our findings that medulloblastomas require Aspm for typical growth suggest that Aspm could be therapeutically targeted to increase the efficacy of radiation and chemotherapy for medulloblastoma. Primary mouse medulloblastoma with *Aspm* deletion provides an ideal model in which to test this possibility in preclinical studies.

MATERIALS AND METHODS

Mice

Aspm-GFP reporter mice [Tg(Aspm-EGFP)IH113Gsat/Mmucd] and *Aspm-CreER* mice are previously described (Gong et al., 2010; Marinaro et al., 2011). For lineage tracing, *Aspm-CreER* mice were crossed with *Rosa26-Lox-STOP-Lox-TdTomato* (Madisen et al., 2010) reporter mice (strain#7914; Jackson Laboratories). Tamoxifen (275 µg in 25 µl sunflower oil) was injected intraperitoneally into *Aspm-CreER;tdTomato* mice and *TdTomato* littermate controls lacking *Aspm-CreER*, at the indicated ages.

$Aspm^{SA/SA}$ mice were generated from *Aspm*-targeted embryonic stem cells (line EPD0320_1_A06, $Aspm^{Gt(KOMP)Wtsi}$; KOMP Repository, Davis, CA, USA). The targeting vector is described in Fig. S2. Generation of $Aspm^{SA/SA}$, *Aspm* cKO and *hGFAP-Cre;SmoM2;*$Aspm^{f/f}$ mice are detailed in supplementary Materials and Methods.

Medulloblastoma-prone *NeuroD2:SmoA1* mice are previously described (Hallahan et al., 2004). *Bax* floxed mice were derived from the $Bax^{f/f}$;$Bak^{-/-}$ strain (Takeuchi et al., 2005) crossed with C57BL/6 to recover wild-type *Bak*. Conditional *p53* (Jonkers et al., 2001) were provided by the NCI (strain#01XC2, Frederick, MD, USA). The *SmoM2*, *SmoA1*, $Bax^{f/f}$, $Trp53^{f/f}$ and all Cre-expressing lines were crossed through at least four generations into a C57BL/6 genetic background. All animal handling and protocols were carried out in accordance with established NIH practices and approved under UNC IACUC# 10-126.

CGNP culture

CGNPs were isolated and explanted as previously described (Kenney et al., 2003) and maintained in 0.5 µg/ml Shh (R&D Systems) or vehicle (0.5% BSA in PBS).

RNA isolation and quantitative real-time PCR (RT-qPCR)

Total RNA was isolated from cerebella or explanted CGNPs using the RNeasy kit (Qiagen), and cDNA synthesized from 1 µg total RNA using Superscript III (Invitrogen/Life Technologies). Gene expression was quantified on an ABI PRISM 7500 Sequence Detection System, using the $\Delta\Delta C_T$ relative quantification method. All experiments included no template controls and were performed in triplicate and repeated twice independently. Primer sequences are listed in supplementary Materials and Methods.

In vivo proliferation analysis

Mice were injected intraperitoneally at the indicated ages with 50 µl Hanks' Balanced Salt Solution containing EdU or BrdU (250 µM, Invitrogen). After the indicated interval, brains were dissected and fixed in 4% formaldehyde in PBS for 24 h at 4°C, then processed for histology.

Histology, immunochemistry and quantification and MRI

Mouse brains were processed and *in situ* hybridization and immunohistochemistry were performed as previously described (Gershon et al., 2009, 2013; Garcia et al., 2012), using the *Aspm* probe (Advanced Cell Diagnostics, #318711) or primary antibodies listed in supplementary Materials and Methods. Methods for quantitative analysis of mitosis, spindle orientation, BrdU/p27, cC3, γH2AX, tumor size and volumetric MRI are detailed in supplementary Materials and Methods. ITK-Snap software (www.itksnap.org) was used to isolate the cerebellar region in MR images (Yushkevich et al., 2006). TUNEL was performed using the Click-iT TUNEL Kit (Life Technologies, #C10245).

Western blot analysis

Whole cerebella were processed as previously described (Garcia et al., 2012) using primary antibodies to γH2AX and β-actin (Cell Signaling, #4970).

Acknowledgements

We thank Luca Muzio (San Raffaele Scientific Institute, Milan, Italy) for *Aspm-CreER* mice, GENSAT for *Aspm-GFP* mice, David Rowitch, (UCSF, CA, USA) and Robert Wechsler-Reya (Sanford-Burnham Medical Research Institute, La Jolla, CA, USA) for *Math1-Cre* mice, Eva Anton (UNC, Chapel Hill, NC, USA) for *hGFAP-Cre* mice, and James Olson (Fred Hutchinson Cancer Research Center, Seattle, WA, USA) for

NeuroD2:SmoA1 mice. We thank the UNC Small Animal Imaging and Tissue Pathology Laboratory Core facilities for providing the MR imaging and immunohistochemistry.

Competing interests
The authors declare no competing or financial interests.

Author contributions
Experiments were conceived by I.G., S.E.W. and T.R.G. Experiments were performed by I.G., S.E.W., A.J.C., A.S., S.L., S.O., K.V., J.R.M. and H.L. Data were analyzed by S.E.W., I.G., K.J.L., S.O., E.A.O., Y.-Y.I.S., K.V. and T.R.G. Manuscript was written by I.G., S.E.W. and T.R.G., with input from all authors.

Funding
S.W. is supported by the Sidney Kimmel Foundation for Cancer Research [SKF-15-065] and an IBM Junior Faculty Development Award. I.G. is supported by the US Department of Defense Congressionally Directed Medical Research Program [CA110045]. Y.-Y.I.S. is supported by the National Institute of Neurological Disorders and Stroke (NINDS) [R01NS091236], the American Heart Association [15SDG23260025] and the Brain and Behavior Foundation. T.R.G. is supported by the NINDS [K08NS077978, R01NS088219], St. Baldrick's Foundation, Morgan Adams Foundation, American Institute for Cancer Research, and Matthew Larson Brain Tumor Foundation. Deposited in PMC for release after 12 months.

Supplementary information
Supplementary information available online at
http://dev.biologists.org/lookup/suppl/doi:10.1242/dev.124271/-/DC1

References
Adachi, Y., Mochida, G., Walsh, C. and Barkovich, J. (2014). Posterior fossa in primary microcephaly: relationships between forebrain and mid-hindbrain size in 110 patients. *Neuropediatrics* **45**, 93-101.
Bazzi, H. and Anderson, K. V. (2014). Acentriolar mitosis activates a p53-dependent apoptosis pathway in the mouse embryo. *Proc. Natl. Acad. Sci. USA* **111**, E1491-E1500.
Bikeye, S.-N., Colin, C., Marie, Y., Vampouille, R., Ravassard, P., Rousseau, A., Boisselier, B., Idbaih, A., Calvo, C. F., Leuraud, P. et al. (2010). ASPM-associated stem cell proliferation is involved in malignant progression of gliomas and constitutes an attractive therapeutic target. *Cancer Cell Int.* **10**, 1.
Bond, J., Roberts, E., Mochida, G. H., Hampshire, D. J., Scott, S., Askham, J. M., Springell, K., Mahadevan, M., Crow, Y. J., Markham, A. F. et al. (2002). ASPM is a major determinant of cerebral cortical size. *Nat. Genet.* **32**, 316-320.
Bond, J., Scott, S., Hampshire, D. J., Springell, K., Corry, P., Abramowicz, M. J., Mochida, G. H., Hennekam, R. C. M., Maher, E. R., Fryns, J.-P. et al. (2003). Protein-truncating mutations in ASPM cause variable reduction in brain size. *Am. J. Hum. Genet.* **73**, 1170-1177.
Brüning-Richardson, A., Bond, J., Alsiary, R., Richardson, J., Cairns, D. A., McCormack, L., Hutson, R., Burns, P., Wilkinson, N., Hall, G. D. et al. (2011). ASPM and microcephalin expression in epithelial ovarian cancer correlates with tumour grade and survival. *Br. J. Cancer* **104**, 1602-1610.
Caldas, H., Jiang, Y., Holloway, M. P., Fangusaro, J., Mahotka, C., Conway, E. M. and Altura, R. A. (2005). Survivin splice variants regulate the balance between proliferation and cell death. *Oncogene* **24**, 1994-2007.
Chong, M. J., Murray, M. R., Gosink, E. C., Russell, H. R. C., Srinivasan, A., Kapsetaki, M., Korsmeyer, S. J. and McKinnon, P. J. (2000). Atm and Bax cooperate in ionizing radiation-induced apoptosis in the central nervous system. *Proc. Natl. Acad. Sci. USA* **97**, 889-894.
Crowther, A. J., Gama, V., Bevilacqua, A., Chang, S. X., Yuan, H., Deshmukh, M. and Gershon, T. R. (2013). Tonic activation of Bax primes neural progenitors for rapid apoptosis through a mechanism preserved in medulloblastoma. *J. Neurosci.* **33**, 18098-18108. in press.
Dahmane, N. and Ruiz-i-Altaba, A. (1999). Sonic hedgehog regulates the growth and patterning of the cerebellum. *Development* **126**, 3089-3100.
Ellison, D. W., Dalton, J., Kocak, M., Nicholson, S. L., Fraga, C., Neale, G., Kenney, A. M., Brat, D. J., Perry, A., Yong, W. H. et al. (2011). Medulloblastoma: clinicopathological correlates of SHH, WNT, and non-SHH/WNT molecular subgroups. *Acta Neuropathol.* **121**, 381-396.
Espinosa, J. S. and Luo, L. (2008). Timing neurogenesis and differentiation: insights from quantitative clonal analyses of cerebellar granule cells. *J. Neurosci.* **28**, 2301-2312.
Farley, F. W., Soriano, P., Steffen, L. S. and Dymecki, S. M. (2000). Widespread recombinase expression using FLPeR (flipper) mice. *Genesis* **28**, 106-110.
Fish, J. L., Kosodo, Y., Enard, W., Paabo, S. and Huttner, W. B. (2006). Aspm specifically maintains symmetric proliferative divisions of neuroepithelial cells. *Proc. Natl. Acad. Sci. USA* **103**, 10438-10443.
Fridman, J. S. and Lowe, S. W. (2003). Control of apoptosis by p53. *Oncogene* **22**, 9030-9040.
Fujita, S. (1967). Quantitative analysis of cell proliferation and differentiation in the cortex of the postnatal mouse cerebellum. *J. Cell Biol.* **32**, 277-287.
Garcia, I., Crowther, A. J., Gama, V., Ryan Miller, C., Deshmukh, M. and Gershon, T. R. (2012). Bax deficiency prolongs cerebellar neurogenesis, accelerates medulloblastoma formation and paradoxically increases both malignancy and differentiation. *Oncogene*. **32**, 2304-2314.
Gershon, T. R., Shirazi, A., Qin, L.-X., Gerald, W. L., Kenney, A. M. and Cheung, N.-K. (2009). Enteric neural crest differentiation in ganglioneuromas implicates hedgehog signaling in peripheral neuroblastic tumor pathogenesis. *PLoS ONE* **4**, e7491.
Gershon, T. R., Crowther, A. J., Liu, H., Miller, C. R. and Deshmukh, M. (2013). Cerebellar granule neuron progenitors are the source of Hk2 in the postnatal cerebellum. *Cancer Metabol.* **1**, 15.
Gong, S., Kus, L. and Heintz, N. (2010). Rapid bacterial artificial chromosome modification for large-scale mouse transgenesis. *Nat. Protoc.* **5**, 1678-1696.
Hallahan, A. R., Pritchard, J. I., Hansen, S., Benson, M., Stoeck, J., Hatton, B. A., Russell, T. L., Ellenbogen, R. G., Bernstein, I. D., Beachy, P. A. et al. (2004). The SmoA1 mouse model reveals that notch signaling is critical for the growth and survival of sonic hedgehog-induced medulloblastomas. *Cancer Res.* **64**, 7794-7800.
Hatten, M. E., Rifkin, D. B., Furie, M. B., Mason, C. A. and Liem, R. K. (1982). Biochemistry of granule cell migration in developing mouse cerebellum. *Prog. Clin. Biol. Res.* **85B**, 509-519.
Hatton, B. A., Villavicencio, E. H., Tsuchiya, K. D., Pritchard, J. I., Ditzler, S., Pullar, B., Hansen, S., Knoblaugh, S. E., Lee, D., Eberhart, C. G. et al. (2008). The Smo/Smo model: hedgehog-induced medulloblastoma with 90% incidence and leptomeningeal spread. *Cancer Res.* **68**, 1768-1776.
Helms, A. W., Abney, A. L., Ben-Arie, N., Zoghbi, H. Y. and Johnson, J. E. (2000). Autoregulation and multiple enhancers control Math1 expression in the developing nervous system. *Development* **127**, 1185-1196.
Hibi, M. and Shimizu, T. (2012). Development of the cerebellum and cerebellar neural circuits. *Dev. Neurobiol.* **72**, 282-301.
Higgins, J., Midgley, C., Bergh, A.-M., Bell, S. M., Askham, J. M., Roberts, E., Binns, R. K., Sharif, S. M., Bennett, C., Glover, D. M. et al. (2010). Human ASPM participates in spindle organisation, spindle orientation and cytokinesis. *BMC Cell Biol.* **11**, 85.
Horvath, S., Zhang, B., Carlson, M., Lu, K. V., Zhu, S., Felciano, R. M., Laurance, M. F., Zhao, W., Qi, S., Chen, Z. et al. (2006). Analysis of oncogenic signaling networks in glioblastoma identifies ASPM as a molecular target. *Proc. Natl. Acad. Sci. USA* **103**, 17402-17407.
Houlihan, S. L. and Feng, Y. (2014). The scaffold protein Nde1 safeguards the brain genome during S phase of early neural progenitor differentiation. *eLife* **3**, e03297.
Jonkers, J., Meuwissen, R., van der Gulden, H., Peterse, H., van der Valk, M. and Berns, A. (2001). Synergistic tumor suppressor activity of BRCA2 and p53 in a conditional mouse model for breast cancer. *Nat. Genet.* **29**, 418-425.
Kaindl, A. M., Passemard, S., Kumar, P., Kraemer, N., Issa, L., Zwirner, A., Gerard, B., Verloes, A., Mani, S. and Gressens, P. (2010). Many roads lead to primary autosomal recessive microcephaly. *Prog. Neurobiol.* **90**, 363-383.
Kato, T. A., Okayasu, R., Jeggo, P. A. and Fujimori, A. (2011). ASPM influences DNA double-strand break repair and represents a potential target for radiotherapy. *Int. J. Radiat. Biol.* **87**, 1189-1195.
Kenney, A. M. and Rowitch, D. H. (2000). Sonic hedgehog promotes G1 cyclin expression and sustained cell cycle progression in mammalian neuronal precursors. *Mol. Cell. Biol.* **20**, 9055-9067.
Kenney, A. M., Cole, M. D. and Rowitch, D. H. (2003). Nmyc upregulation by sonic hedgehog signaling promotes proliferation in developing cerebellar granule neuron precursors. *Development* **130**, 15-28.
Kim, H.-T., Lee, M.-S., Choi, J.-H., Jung, J.-Y., Ahn, D.-G., Yeo, S.-Y., Choi, D.-K. and Kim, C.-H. (2011). The microcephaly gene aspm is involved in brain development in zebrafish. *Biochem. Biophys. Res. Commun.* **409**, 640-644.
Kuang, Y., Liu, Q., Shu, X., Zhang, C., Huang, N., Li, J., Jiang, M. and Li, H. (2012). Dicer1 and MiR-9 are required for proper Notch1 signaling and the Bergmann glial phenotype in the developing mouse cerebellum. *Glia* **60**, 1734-1746.
Lee, Y. and McKinnon, P. J. (2007). Responding to DNA double strand breaks in the nervous system. *Neuroscience* **145**, 1365-1374.
Lee, Y., Shull, E. R. P., Frappart, P.-O., Katyal, S., Enriquez-Rios, V., Zhao, J., Russell, H. R., Brown, E. J. and McKinnon, P. J. (2012). ATR maintains select progenitors during nervous system development. *EMBO J.* **31**, 1177-1189.
Lin, S.-Y., Pan, H.-W., Liu, S.-H., Jeng, Y.-M., Hu, F.-C., Peng, S.-Y., Lai, P.-L. and Hsu, H.-C. (2008). ASPM is a novel marker for vascular invasion, early recurrence, and poor prognosis of hepatocellular carcinoma. *Clin. Cancer Res.* **14**, 4814-4820.
Lizarraga, S. B., Margossian, S. P., Harris, M. H., Campagna, D. R., Han, A. P., Blevins, S., Mudbhary, R., Barker, J. E., Walsh, C. A. and Fleming, M. D. (2010). Cdk5rap2 regulates centrosome function and chromosome segregation in neuronal progenitors. *Development* **137**, 1907-1917.
Machold, R. and Fishell, G. (2005). Math1 is expressed in temporally discrete pools of cerebellar rhombic-lip neural progenitors. *Neuron* **48**, 17-24.

Development (2015) 142, 3921-3932 doi:10.1242/dev.124271

Madisen, L., Zwingman, T. A., Sunkin, S. M., Oh, S. W., Zariwala, H. A., Gu, H., Ng, L. L., Palmiter, R. D., Hawrylycz, M. J., Jones, A. R. et al. (2010). A robust and high-throughput Cre reporting and characterization system for the whole mouse brain. *Nat. Neurosci.* **13**, 133-140.

Mao, J., Ligon, K. L., Rakhlin, E. Y., Thayer, S. P., Bronson, R. T., Rowitch, D. and McMahon, A. P. (2006). A novel somatic mouse model to survey tumorigenic potential applied to the hedgehog pathway. *Cancer Res.* **66**, 10171-10178.

Marinaro, C., Butti, E., Bergamaschi, A., Papale, A., Furlan, R., Comi, G., Martino, G. and Muzio, L. (2011). In vivo fate analysis reveals the multipotent and self-renewal features of embryonic AspM expressing cells. *PLoS ONE* **6**, e19419.

Matei, V., Pauley, S., Kaing, S., Rowitch, D., Beisel, K. W., Morris, K., Feng, F., Jones, K., Lee, J. and Fritzsch, B. (2005). Smaller inner ear sensory epithelia in Neurog1 null mice are related to earlier hair cell cycle exit. *Dev. Dyn.* **234**, 633-650.

Montgomery, S. H. and Mundy, N. I. (2014). Microcephaly genes evolved adaptively throughout the evolution of eutherian mammals. *BMC Evol. Biol.* **14**, 120.

Nakashima, K., Umeshima, H. and Kengaku, M. (2015). Cerebellar granule cells are predominantly generated by terminal symmetric divisions of granule cell precursors. *Dev. Dyn.* **244**, 748-758.

Northcott, P. A., Korshunov, A., Witt, H., Hielscher, T., Eberhart, C. G., Mack, S., Bouffet, E., Clifford, S. C., Hawkins, C. E., French, P. et al. (2011). Medulloblastoma comprises four distinct molecular variants. *J. Clin. Oncol.* **29**, 1408-1414.

Novorol, C., Burkhardt, J., Wood, K. J., Iqbal, A., Roque, C., Coutts, N., Almeida, A. D., He, J., Wilkinson, C. J. and Harris, W. A. (2013). Microcephaly models in the developing zebrafish retinal neuroepithelium point to an underlying defect in metaphase progression. *Open Biol.* **3**, 130065.

Paramasivam, M., Chang, Y. J. and LoTurco, J. J. (2007). ASPM and citron kinase co-localize to the midbody ring during cytokinesis. *Cell Cycle* **6**, 1605-1612.

Pawlisz, A. S., Mutch, C., Wynshaw-Boris, A., Chenn, A., Walsh, C. A. and Feng, Y. (2008). Lis1-Nde1-dependent neuronal fate control determines cerebral cortical size and lamination. *Hum. Mol. Genet.* **17**, 2441-2455.

Poulton, J. S., Cuningham, J. C. and Peifer, M. (2014). Acentrosomal Drosophila epithelial cells exhibit abnormal cell division, leading to cell death and compensatory proliferation. *Dev. Cell* **30**, 731-745.

Pulvers, J. N., Bryk, J., Fish, J. L., Wilsch-Brauninger, M., Arai, Y., Schreier, D., Naumann, R., Helppi, J., Habermann, B., Vogt, J. et al. (2010). Mutations in mouse Aspm (abnormal spindle-like microcephaly associated) cause not only microcephaly but also major defects in the germline. *Proc. Natl. Acad. Sci. USA* **107**, 16595-16600.

Riparbelli, M. G., Callaini, G., Glover, D. M. and Avides Mdo, C. (2002). A requirement for the Abnormal Spindle protein to organise microtubules of the central spindle for cytokinesis in Drosophila. *J. Cell Sci.* **115**, 913-922.

Roussel, M. F. and Hatten, M. E. (2011). Cerebellum: development and medulloblastoma. *Curr. Top. Dev. Biol.* **94**, 235-282.

Rubin, L. L. and de Sauvage, F. J. (2006). Targeting the Hedgehog pathway in cancer. *Nat. Rev. Drug Discov.* **5**, 1026-1033.

Rujano, M. A., Sanchez-Pulido, L., Pennetier, C., le Dez, G. and Basto, R. (2013). The microcephaly protein Asp regulates neuroepithelium morphogenesis by controlling the spatial distribution of myosin II. *Nat. Cell Biol.* **15**, 1294-1306.

Saunders, R. D. C., Avides, M. d. C., Howard, T., Gonzalez, C. and Glover, D. M. (1997). The Drosophila gene abnormal spindle encodes a novel microtubule-associated protein that associates with the polar regions of the mitotic spindle. *J. Cell Biol.* **137**, 881-890.

Schilling, K., Oberdick, J., Rossi, F. and Baader, S. L. (2008). Besides Purkinje cells and granule neurons: an appraisal of the cell biology of the interneurons of the cerebellar cortex. *Histochem. Cell Biol.* **130**, 601-615.

Schüller, U., Heine, V. M., Mao, J., Kho, A. T., Dillon, A. K., Han, Y.-G., Huillard, E., Sun, T., Ligon, A. H., Qian, Y. et al. (2008). Acquisition of granule neuron precursor identity is a critical determinant of progenitor cell competence to form Shh-induced medulloblastoma. *Cancer Cell* **14**, 123-134.

Silver, D. L., Watkins-Chow, D. E., Schreck, K. C., Pierfelice, T. J., Larson, D. M., Burnetti, A. J., Liaw, H.-J., Myung, K., Walsh, C. A., Gaiano, N. et al. (2010). The exon junction complex component Magoh controls brain size by regulating neural stem cell division. *Nat. Neurosci.* **13**, 551-558.

Takeuchi, O., Fisher, J., Suh, H., Harada, H., Malynn, B. A. and Korsmeyer, S. J. (2005). Essential role of BAX,BAK in B cell homeostasis and prevention of autoimmune disease. *Proc. Natl. Acad. Sci. USA* **102**, 11272-11277.

van der Voet, M., Berends, C. W. H., Perreault, A., Nguyen-Ngoc, T., Gönczy, P., Vidal, M., Boxem, M. and van den Heuvel, S. (2009). NuMA-related LIN-5, ASPM-1, calmodulin and dynein promote meiotic spindle rotation independently of cortical LIN-5/GPR/Galpha. *Nat. Cell Biol.* **11**, 269-277.

Vousden, K. H. and Lu, X. (2002). Live or let die: the cell's response to p53. *Nat. Rev. Cancer* **2**, 594-604.

Vulcani-Freitas, T. M., Saba-Silva, N., Cappellano, A., Cavalheiro, S., Marie, S. K. N., Oba-Shinjo, S. M., Malheiros, S. M. F. and de Toledo, S. R. C. (2011). ASPM gene expression in medulloblastoma. *Childs Nerv. Syst.* **27**, 71-74.

Wakefield, J. G., Bonaccorsi, S. and Gatti, M. (2001). The Drosophila protein Asp is involved in microtubule organization during spindle formation and cytokinesis. *J. Cell Biol.* **153**, 637-648.

Wang, W.-Y., Hsu, C.-C., Wang, T.-Y., Li, C.-R., Hou, Y.-C., Chu, J.-M., Lee, C.-T., Liu, M.-S., Su, J. J.-M., Jian, K.-Y. et al. (2013). A gene expression signature of epithelial tubulogenesis and a role for ASPM in pancreatic tumor progression. *Gastroenterology* **145**, 1110-1120.

Wechsler-Reya, R. J. and Scott, M. P. (1999). Control of neuronal precursor proliferation in the cerebellum by sonic hedgehog. *Neuron* **22**, 103-114.

Williams, S. E., Beronja, S., Pasolli, H. A. and Fuchs, E. (2011). Asymmetric cell divisions promote Notch-dependent epidermal differentiation. *Nature* **470**, 353-358.

Woods, C. G., Bond, J. and Enard, W. (2005). Autosomal recessive primary microcephaly (MCPH): a review of clinical, molecular, and evolutionary findings. *Am. J. Hum. Genet.* **76**, 717-728.

Yang, Z.-J., Ellis, T., Markant, S. L., Read, T.-A., Kessler, J. D., Bourboulas, M., Schüller, U., Machold, R., Fishell, G., Rowitch, D. H. et al. (2008). Medulloblastoma can be initiated by deletion of patched in lineage-restricted progenitors or stem cells. *Cancer Cell* **14**, 135-145.

Yushkevich, P. A., Piven, J., Hazlett, H. C., Smith, R. G., Ho, S., Gee, J. C. and Gerig, G. (2006). User-guided 3D active contour segmentation of anatomical structures: significantly improved efficiency and reliability. *Neuroimage* **31**, 1116-1128.

Zagon, I. S. and McLaughlin, P. J. (1987). The location and orientation of mitotic figures during histogenesis of the rat cerebellar cortex. *Brain Res. Bull.* **18**, 325-336.

Zhong, X., Liu, L., Zhao, A., Pfeifer, G. P. and Xu, X. (2005). The abnormal spindle-like, microcephaly-associated (ASPM) gene encodes a centrosomal protein. *Cell Cycle* **4**, 1227-1229.

Zhuo, L., Theis, M., Alvarez-Maya, I., Brenner, M., Willecke, K. and Messing, A. (2001). hGFAP-cre transgenic mice for manipulation of glial and neuronal function in vivo. *Genesis* **31**, 85-94.

Zurawel, R. H., Allen, C., Wechsler-Reya, R., Scott, M. P. and Raffel, C. (2000a). Evidence that haploinsufficiency of Ptch leads to medulloblastoma in mice. *Genes Chromosomes Cancer* **28**, 77-81.

Zurawel, R. H., Allen, C., Chiappa, S., Cato, W., Biegel, J., Cogen, P., de Sauvage, F. and Raffel, C. (2000b). Analysis of PTCH/SMO/SHH pathway genes in medulloblastoma. *Genes Chromosomes Cancer* **27**, 44-51.